Domain growth and nucleation in a discrete bistable system

Gian-Luca Oppo and Raymond Kapral
Chemical Physics Theory Group, Department of Chemistry, University of Toronto, Toronto, Ontario, Canada M5S 1A1
(Received 26 June 1987)

A cubic map lattice, which consists of an array of cubic discrete-time maps coupled through nearest-neighbor diffusion interactions, is studied in a parameter region where the isolated maps possess bistable steady states. Within this parameter region, the spatio-temporal evolution of this deterministic dynamical system exhibits the phenomena of phase separation and nucleation. When the two coexisting states have the same stability, the domain growth is like that for continuous systems with a nonconserved order parameter, and follows Allen-Cahn scaling on long distance and time scales. When the states have different stabilities, growth typically occurs by a nucleation process. In addition to exploring these phenomena, which have their analogs in continuous systems, features of the inhomogeneous states peculiar to the discrete model are also investigated.

I. INTRODUCTION

Phase separation and domain growth in nonequilibrium systems are common phenomena in nature, yet many aspects of the description of the dynamics of these processes are not completely understood. Typically, the time evolution of such systems is described in terms of the behavior of an order parameter, which may be either conserved or nonconserved. We restrict our attention to cases where the order parameter is not conserved; thus, we have in mind phenomena like the competition between bistable states in a reaction-diffusion system, the development of domains of staggered magnetization in a ferromagnetic system, or the antiphase boundary motion in some alloys, to mention just a few such processes.[1]

Systems of this type can show rather different kinds of behavior depending on whether the two competing states have the same or different stabilities. In the former case, according to the Allen-Cahn theory,[2] the motion and growth of one phase in the other is governed by the curvature of the domain boundaries, and does not depend on the surface free energy. In this circumstance a planar interface between the phases is stable and will not propagate in space and time. If, on the other hand, one state is more stable than the other, the more-stable phase will grow at the expense of the less-stable phase; the planar interface will move with a constant shape and a constant velocity whose magnitude depends on the stability difference. In general, when the curvature of the interface is taken into account, phase growth can be described by a nucleation process.[3] There have been numerous simulation studies which have attempted to verify various aspects of the theoretical predictions, or probe the dynamics of the above-mentioned processes more deeply.[1]

A class of deterministic discrete-space and discrete-time models comprising cellular automata[4] and coupled map lattices[5] also exhibits phase separation and nucleation phenomena. They are trivial to simulate and amenable to theoretical analysis in some circumstances. The aims of the present paper are to study and document the existence of a variety of phase-separation phenomena, analogous to those in the continuum systems, for a coupled map model possessing bistable steady states.

Section II describes the model and outlines the parameter range within which our study is confined. The nature of the discrete, planar interface is studied in Sec. III and contrasted with the corresponding continuum interface. Domain evolution in two dimensions and effects due to the existence of curved interfaces are the topics considered in Secs. IV and V. Section IV deals with the phase separation of equally stable states, and makes comparisons with the Allen-Cahn theory, while Sec. V considers nucleation processes in situations where the states have different stabilities. The results are discussed in Sec. VI.

II. THE DISCRETE MODEL

The model dynamical system was introduced earlier[6] in an investigation of some aspects of the coexistence of stable states in spatially distributed systems: It consists of a d-dimensional array of N coupled cubic maps,

$$x(\mathbf{i},t+1)=f(x(\mathbf{i},t))+\gamma\left[\sum_{\langle j\rangle}^{q}x(\mathbf{j},t)-qx(\mathbf{i},t)\right], \tag{2.1}$$

with

$$f(x)=-ax^3+(1+\epsilon)x+c\ . \tag{2.2}$$

In Eq. (2.1) $\langle j\rangle$ refers to the sum of the q neighbors of i, but in this paper we restrict our discussions to the case of nearest-neighbor coupling in one or two dimensions where $q=2$ or 4, respectively. Furthermore, we let $a=1$ and consider the behavior as a function of ϵ, c, and the coupling strength γ.

Simulations and linear stability analyses of this model have shown that a wide variety of spatio-temporal structures exist.[6] All of the investigations of domain growth carried out here pertain to the region of the (ϵ,c,γ) parameter surface where two stable homogeneous steady

states coexist. The phase diagram for the relevant parameter region is shown in Fig. 1. If studies of the dynamical behavior are confined to this region of the phase diagram, most of the phenomena exhibited by the discrete space-time model mimic those of the corresponding continuous system. In fact, Eq. (2.1) is simply the discrete version of the time-dependent Ginzburg-Landau (TDGL) model,

$$\dot{x}(\mathbf{r},t)=-a[x(\mathbf{r},t)]^3+\epsilon x(\mathbf{r},t)+c+\gamma\nabla^2 x(\mathbf{r},t)\ , \qquad (2.3)$$

which has been used extensively in theoretical investigations of phase-separation processes.[1] We prefer to regard the coupled map lattice as a model in its own right. The discrete model has a much richer bifurcation structure than Eq. (2.3): for example, while subharmonic bifurcations can take place as the parameters are tuned in the coupled map model, these cannot occur in its continuous counterpart; thus, some care must be used in the application of the model results to physical systems. However, we note that in some instances the physical situation lends itself to modeling by a discrete equation; this is especially true of some biological applications.[7] On the other hand, provided the parameter region is chosen to avoid unwanted bifurcations, the results have a bearing on physical systems whose underlying dynamics is best described by a continuous model.[8] Evidence for this point is given in Secs. IV and V.

The paper is largely concerned with the structure and dynamics of the interface between coexisting stable states. The simplest type of interface to consider is a planar one: the equations of motion reduce to those for a single spatial degree of freedom, and, naturally, complications due to curvature do not enter. Since the nature of the interface determines all the phenomena of interest, we devote the next section to a study of some of the peculiar features of the discrete, planar interface.

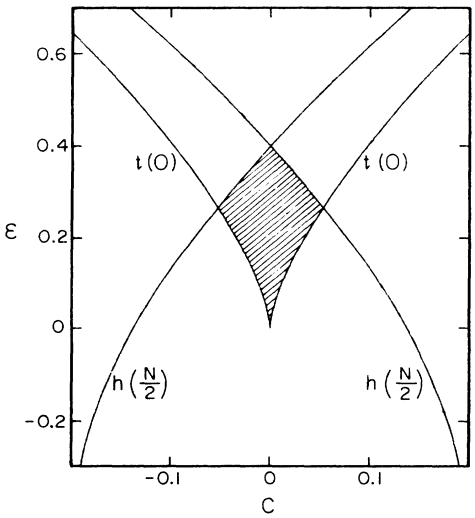

FIG. 1. Phase diagram in the (ϵ,c) parameter plane for $\gamma=0.15$. Within the shaded area two stable steady states coexist. The curve marked t corresponds to a tangent bifurcation where the number of stable states changes. The curve marked h is the first subharmonic bifurcation boundary.

III. STRUCTURE OF THE DISCRETE, PLANAR INTERFACE

Consider a planar interface separating the two phases. If $c=0$ the two phases have identical stability and, in the continuous case, the interface is stable and has a hyperbolic-tangent form. For the discrete model, the planar interface is stable also, and its shape is closely approximated by a hyperbolic tangent, but is not given exactly by this function. Below we study in some detail how the interface arises in the discrete model. The discrete interface has been studied in connection with a different set of physical problems: commensurate-incommensurate phase transitions in metal insulators and pinned solitons.[9] The equations describing these systems also take a form which is similar to that of the coupled cubic map lattice. The analysis presented below focuses on the symmetry properties of the system and their role in determining the structure of the stable interfacial profile. An algorithm is developed for directly computing the profile, and a temporal stability analysis is carried out in order to provide insight into how the interface arises and responds to perturbations. Finally, the generalization to the asymmetric case $c=0$ is discussed, focusing on the peculiarities of the discrete model.

Since the spatial degree of freedom normal to the interface is the only relevant one, we study the stationary, inhomogeneous solutions of Eq. (2.1), with $q=2$ and i a one-dimensional discrete index:

$$x(i+1)=-\gamma^{-1}[f(x(i))-x(i)]-x(i-1)+2x(i)\ . \qquad (3.1)$$

Introducing $y(i)=x(i-1)$, the following two-dimensional area-preserving map with periodic boundary conditions is obtained:

$$\begin{aligned} x(i+1)&=-\gamma^{-1}[f(x(i))-x(i)]+2x(i)-y(i)\\ &=F(x(i))-y(i)\ ,\\ y(i+1)&=x(i)\ , \end{aligned} \qquad (3.2a)$$

which may be written in vector form as

$$\mathbf{r}(i+1)=\mathbf{M}(\mathbf{r}(i))\ . \qquad (3.2b)$$

This map is of the De Vogelaere form,[10] which is manifestly area preserving. One iteration of the map corresponds to a displacement of one lattice spacing along the one-dimensional chain. The solutions of Eq. (3.2) represent all possible stationary profiles for the one-dimensional version of Eq. (2.1).

In the continuous case, a simple integration of the stationary form of Eq. (2.3) is possible, and yields the hyperbolic-tangent profile for the solution connecting the two stable states. Analysis of the discrete model requires other techniques. The fixed point solutions of Eq. (3.2) are given by

$$f(x^*)=x^* \qquad (3.3)$$

and correspond to homogeneous solutions, whose stability can be determined from the eigenvalues of the Jacobian matrix. For $c=0$ and $\gamma>0$, the eigenvalues are

$$\lambda_0^{\pm}=\left[1-\frac{\epsilon}{2\gamma}\right]\pm\left[\frac{\epsilon}{\gamma}\left[\frac{\epsilon}{4\gamma}-1\right]\right]^{1/2} \tag{3.4}$$

for the fixed point $x^*=0$, and

$$\lambda_{1,2}^{\pm}=\left[1+\frac{\epsilon}{\gamma}\right]\pm\left[\frac{\epsilon}{\gamma}\left[\frac{\epsilon}{\gamma}+2\right]\right]^{1/2} \tag{3.5}$$

for the fixed points $x_{1,2}^*=\pm\sqrt{\epsilon}$. The trajectories defined by Eq. (3.2) are shown in Fig. 2 for different values of ϵ and γ. The pictures were obtained by direct iteration of 200 initial conditions equally spaced on the lines $x=y$ or $x=-y$. The results are quite different from those of the corresponding continuous case.[11] Some initial conditions produce closed invariant elliptic curves centered on the origin, but this is true only for $\epsilon<4\gamma$, when $\lambda_0^{\pm}$ are a complex conjugate pair, and $x^*=0$ is an elliptic point. For larger values of ϵ this fixed point undergoes a subharmonic bifurcation, which drastically changes the solution structure [see Fig. 2(d)]. However, even though this behavior may affect the dynamics of the phase separation starting from the unstable state, it has no effect on the stable spatial solutions. The behavior of the map close to the other fixed points, $x_{1,2}^*$, is more relevant to the nature of the discrete interface. For any value of ϵ, both eigenvalues in Eq. (3.5) are real and positive. Moreover, since λ_+ (λ_-) is always larger (smaller) than one, the fixed points are hyperbolic. The boundary layer that connects the two phases is a trajectory of the map which starts from one fixed point and terminates in the other. However, as Fig. 2 shows, the path connecting the two fixed points must thread its way through a chaotic layer. The thickness of this layer depends critically on ϵ and disappears only for $\epsilon=0$. This implies

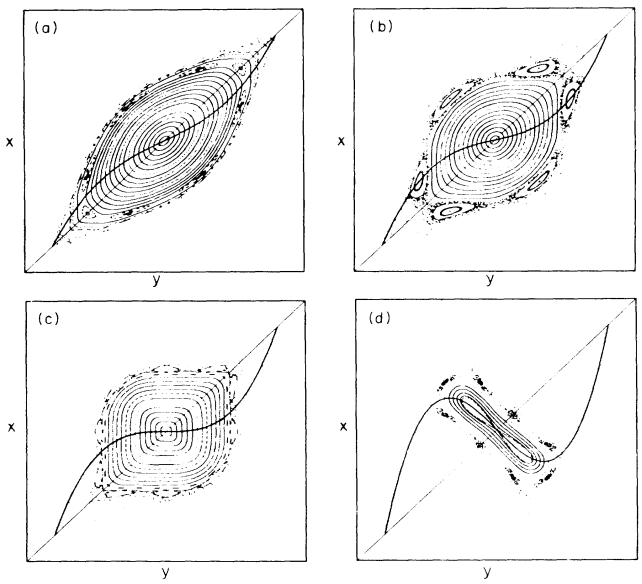

FIG. 2. Conservative map [Eq. (3.2)] for $c=0$ and different values of ϵ and γ: (a) $\epsilon=0.15$, $\gamma=0.15$; (b) $\epsilon=0.23$, $\gamma=0.15$; (c) $\epsilon=0.3$, $\gamma=0.15$; and (d) $\epsilon=0.42$, $\gamma=0.1$. The solid line is the symmetry curve $x=F(y)/2$ whose intersections with the bisectrix are the homogeneous states.

that a smooth "separatrix" connecting the two hyperbolic fixed points does not exist. Nevertheless, a smooth phase boundary profile exists and corresponds to a trajectory through this chaotic layer. The nature of this trajectory can be examined through an investigation of the symmetries associated with the map.

If $\phi(x)$ is an invariant curve under the transformation Eq. (3.2), then

$$F(x)=\phi(x)+\phi^{-1}(x)\ . \tag{3.6}$$

It can be shown[10] that this implies the existence of two symmetry curves, $x=y$, associated with reflection through the bisectrix, and $x=F(y)/2$, associated with reflection through lines parallel to the abscissa. Both curves are shown in Fig. 2. However the closed invariant curves show an additional symmetry with respect to $x=-y$; this symmetry does not exist for the open curves, and is expected in the physics of the problem as a consequence of the equal stability of the two coexisting states for $c=0$. Imposing the latter symmetry in Eq. (3.2), the number of possible orbits describing the interface is reduced to two: the orbit passing through the line $x=-y$, which is represented by

$$-x(-n)=x(n+1),\quad n\geq 0\ , \tag{3.7}$$

and the orbit passing through the lines $x=0$ and $y=0$,

$$-x(-n)=x(n),\quad n\geq 0\ . \tag{3.8}$$

It is possible to give a graphical representation of such orbits by simply iterating the map, Eq. (3.2), in the neighborhood of the hyperbolic fixed points. The stable and unstable manifolds associated with these fixed points can be obtained by iterating a set of points lying along the eigenvectors,

$$\hat{\mathbf{e}}_{\pm}=\begin{bmatrix}\lambda_{\pm}\\ 1\end{bmatrix} \tag{3.9}$$

and slightly displaced from the fixed points. Figure 3 presents a sample of the manifolds for different values of ϵ and γ. The "supersymmetric" orbits given by Eqs. (3.7) and (3.8), which are indicated in Fig. 3(a) by squares and crosses, respectively, correspond to the intersection of the stable manifold of one fixed point with the unstable of the other one; i.e., they are heteroclinic points. The two different paths are sketched in Fig. 3, and show that the relative slopes of the manifolds remain constant at the intersection points for each of the supersymmetric orbits. The system selects the "smooth" symmetric orbits that allow an iterate of Eq. (3.2) to travel from one phase to the other through the chaotic layer.

We next present an algorithm to numerically evaluate the intersections between the two manifolds. Starting in the neighborhood of either fixed point along the expanding direction, an iterate of the conservative map will eventually cross the particular lines on which the supersymmetric orbits lie. We want to determine the point $\hat{\mathbf{r}}$ whose nth iteration lies exactly on a symmetry line and is thus a point on a supersymmetric orbit. Given an initial point $\mathbf{r}_0$ near the fixed point and along an eigenvec-

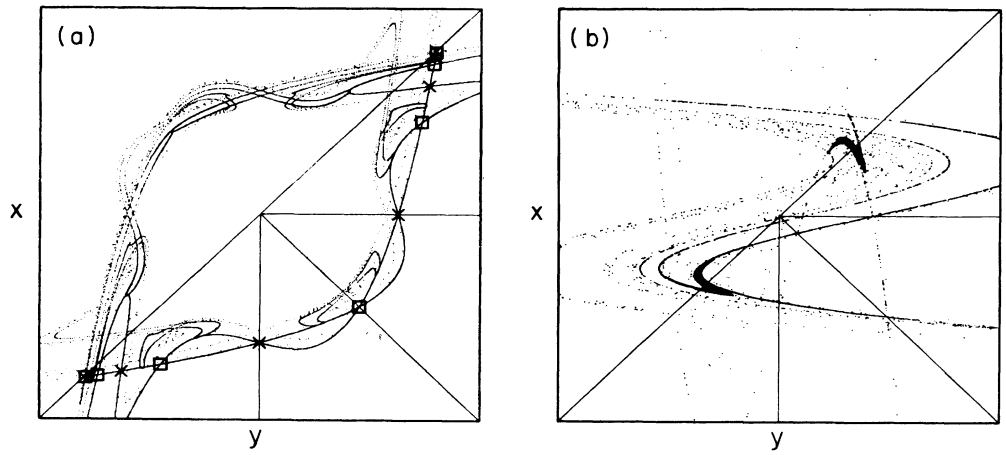

FIG. 3. Unstable manifold of the upper hyperbolic fixed point and the stable manifold of the lower for $c=0$. The intersections indicated by squares and crosses correspond to the orbits (3.7) and (3.8), respectively. (a) $\epsilon=0.3$, $\gamma=0.15$; (b) $\epsilon=0.31$, $\gamma=-0.15$.

tor, we may determine $\delta\mathbf{r}$ necessary to bring this point into coincidence with $\hat{\mathbf{r}}$:

$$\mathbf{r}_0=\hat{\mathbf{r}}+\delta\mathbf{r} \ . \tag{3.10}$$

Of course, $\delta\mathbf{r}$ is again a displacement along the eigendirection, and may be obtained via the linearization

$$\delta\mathbf{r}=[\mathbf{M}'(\mathbf{r}_0)\cdots\mathbf{M}'(\mathbf{r}_{n-2})\mathbf{M}'(\mathbf{r}_{n-1})]^{-1} \times[\mathbf{M}^{(n)}(\mathbf{r}_0)-\mathbf{M}^{(n)}(\hat{\mathbf{r}})] \tag{3.11}$$

where $\mathbf{M}'(\mathbf{r}_m)$ is the matrix of derivatives of the map Eq. (3.2) evaluated at the mth iteration. A few iterations of Eq. (3.11) yield the desired intercept. This method is quite general and is independent of the choice of the surface crossed by the orbit [for the supersymmetric orbit of Eq. (3.8) one has to choose $x=-y$, while for Eq. (3.7) the surface is determined by $y=0$], and the specific form of the map.[12]

Only one of the two supersymmetric stationary solutions is stable (cf. Ref. 9 for a discussion of these "pinned" states in another context), as can be verified by a temporal stability analysis of these orbits. The linearized version of Eq. (2.1) is

$$\delta\mathbf{x}(t+1)=\mathbf{A}\,\delta\mathbf{x}(t) \ , \tag{3.12}$$

where $\mathbf{x}$ is a column vector with elements $x(i,t)$, and the matrix $\mathbf{A}$ has nonzero elements,

$$\begin{aligned} &A(i,i)=-3x(i)^2+(\epsilon+1)-2\gamma \ , \\ &A(i,i-1)=A(i+1,i)=A(1,N)=A(N,1)=\gamma \ . \end{aligned} \tag{3.13}$$

The eigenvalues and eigenvectors of $\mathbf{A}$ were calculated, utilizing the profile elements $x(i)$ obtained from the Newton method described previously. In Fig. 4 the largest eigenvalue for the two supersymmetric orbits is reported as a function of ϵ and γ. The profile generated by the orbit of Eq. (3.7) is temporally stable, and corresponds to all the simulations reported in Fig. 2 of Ref. 6.[13] The orbit of Eq. (3.8), on the other hand, is always unstable, although the magnitude of the largest eigenvalue is only slightly larger than unity. This is the origin of two characteristic time scales in the system: The first

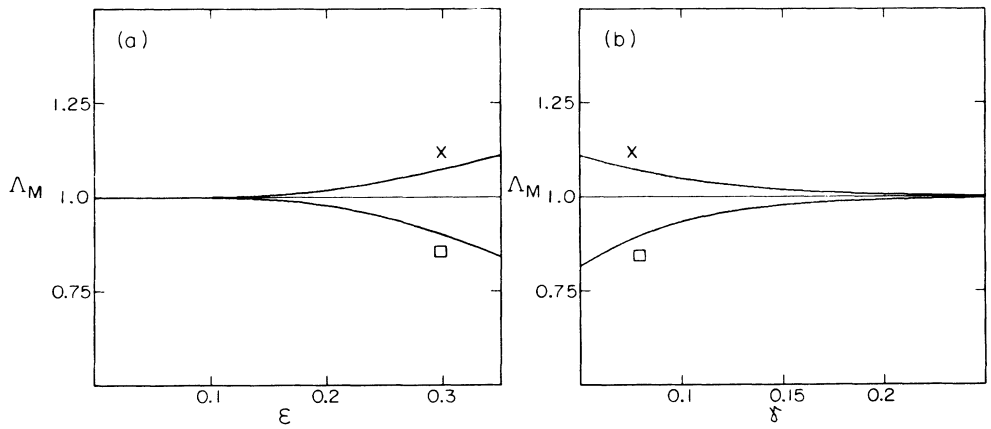

FIG. 4. Largest eigenvalue Λ_M of the temporal stability analysis for the supersymmetric orbits (3.7) (lower line) and (3.8) (upper line) as (a) a function of ϵ for $\gamma=0.15$ and as (b) a function of γ for $\epsilon=0.2$.

time scale corresponds to a fast relaxation (few time steps) of an arbitrary "kinked" initial condition to a state close to one of the two supersymmetric orbits, the second time scale corresponds to the relaxation of the orbit of Eq. (3.8) towards the profile described by Eq. (3.7); this time scale is characterized by the eigenvalues shown in Fig. 4.

More information about the nature of the instability of the trajectory of Eq. (3.8) can be obtained from the distribution of the entire set of eigenvalues and from the corresponding eigenvectors. Figure 5 shows the eigenvalues, ordered by magnitude, of the two supersymmetric orbits for $\epsilon=0.25$ and $\gamma=0.15$. The tails of the curves are independent of the orbit considered, and these small-magnitude eigenvalues are simply those that are found from a linear stability analysis of the inphase solution.[5(a)]

$$\Lambda(j)=f'(x^*)-4\gamma\sin^2\left[\frac{\pi j}{N}\right]. \tag{3.14}$$

Here the index j labels the wavenumbers of the Fourier modes ($0\le j\le N/2$). In Fig. 5 comparison between Eq. (3.14) and the numerical evaluation of the eigenvalues is presented. Only few eigenvalues are larger than $\Lambda(N/2)$ showing that the stability or instability of the orbits is mainly determined by the interfacial region. Figure 6 reports the eigenvectors associated with the interface for the unstable supersymmetric orbit. The largest eigenvalue has a symmetric eigenvector, strongly peaked at the center of the interface, suggesting that the origin of the instability resides in the peculiar behavior of the orbit of Eq. (3.8) in the neighborhood of $x=0$; any perturbation of this point will break the supersymmetry, $x=-y$, and the perturbation will grow in time until the profile described by Eq. (3.7) is reached.

The theory discussed up to this point has dealt only with the equal stability case ($c=0$), which possesses an obvious symmetry in the exchange of the fixed points. The one-dimensional analysis of the continuous equation (2.3) (Ref. 11) shows that for any value of c different from zero the interface front will travel in space until a uniform state of the more-stable phase is restored. This is due to the absence of a separatix connecting the two hyperbolic fixed points for every value of $c\neq 0$. The situation is quite different for the discrete case. The symmetry with respect to $x=-y$ is destroyed, reflecting the different stabilities of the fixed points; however, the intersections between the stable manifold of one fixed point and the unstable of the other one survive for small values of c, and solutions which show similar behavior (but not the same symmetry) to Eqs. (3.7) and (3.8) can still be found. This allows one to recover a stationary profile. As the plots in Fig. 7 show, the intersections gradually approach each other, and for a critical value of c that depends on ϵ the solutions connecting the two stable states disappear when the curves cease to intersect. This corresponds to an inverse tangent bifurcation at which the stable and the unstable orbits analogous to Eqs. (3.7) and (3.8) collide. This picture is confirmed by the temporal linear stability analysis, which shows that

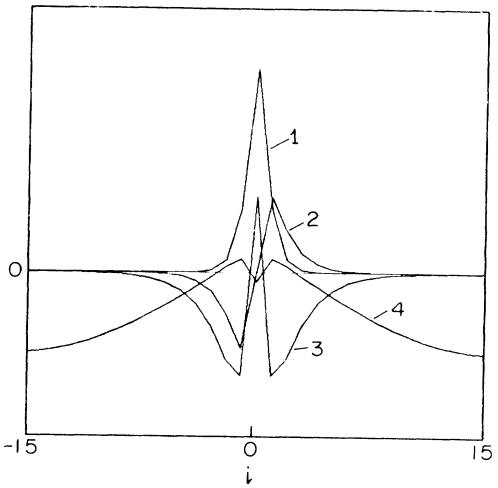

FIG. 6. Eigenvectors of the unstable profile (3.8). The numbers indicate the magnitudes of the corresponding eigenvalues with 1 having the largest magnitude. The ordinate scale is arbitrary.

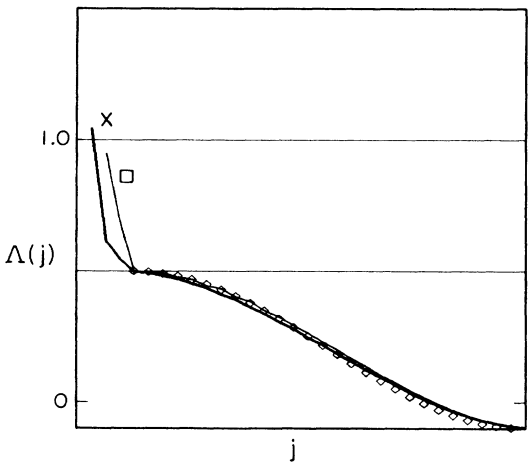

FIG. 5. Eigenvalue distribution for the temporal stability analysis for the stable (light line) and unstable (heavy line) profiles [Eqs. (3.7) and (3.8)] for $\epsilon=0.25$ and $\gamma=0.15$. The squares are the eigenvalues of the homogeneous solution evaluated using Eq. (3.14).

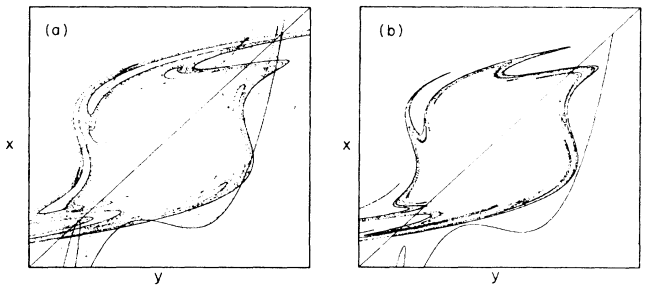

FIG. 7. Same as Fig. 3 but for (a) $c=0.004$ and (b) $c=0.007$. The disappearance of a stable intersection occurs via a tangent collision with a neighboring unstable intersection.

at the critical point the largest eigenvalues for both orbits are equal to unity. For any larger value of c the profile connecting the two states will move, on the average, at a constant velocity (see Sec. V).

A different situation is found for negative values of γ. The two eigenvalues [Eq. (3.5)] form a complex-conjugate pair for

$$\epsilon < 2 | \gamma | \ , \tag{3.15}$$

giving rise to elliptic fixed points; it is now impossible for a phase point to move from one fixed point to the other. Moreover, a linear stability analysis shows that in such a region of the parameter space only period-one spatially alternating solutions are stable, due to the existence of a short wavelength instability.[6] When $\epsilon = 2 | \gamma |$ the elliptic fixed points undergo a subharmonic bifurcation and become hyperbolic. Figure 3(b) shows the stable and unstable manifolds of the hyperbolic fixed points of map, Eq. (3.2), for $\epsilon > 2 | \gamma |$. None of the structure found for negative values of γ has an analog in the continuous model.

It is important to note that the effects described in this section are connected to the fact that the system described by Eq. (2.1) has discrete spatial variables, and not on the specific form (invertible or not) of the map.

IV. PHASE SEPARATION FOR EQUALLY STABLE STATES

In this section we study the dynamics of the phase-separation process in the discrete model for $c = 0$ where the two coexisting fixed points have equal stabilities. We consider the time evolution following a critical quench in which the temperature (the ϵ parameter) is suddenly changed below the critical point ($\epsilon = c = 0$). The lattice is initially prepared in the unstable state $[x(i,j) = 0, \forall i,j]$ to which small fluctuations are added in order to simulate the internal noise of the physical system. The spatial competition between the two phases leads to the growth of clusters of one phase in the other.

Many of the consequences of the Allen-Cahn[2] theory for the motion of curved boundaries in a system with a nonconserved order parameter have been checked in Monte Carlo (MC) simulations of Ising models.[1] We show below that most aspects of the curved boundary evolution in the cubic map lattice are in accord with this theory.

In the phase-separation process any curved boundary separating the two different phases moves with a velocity v given by

$$v = -\gamma K \ , \tag{4.1}$$

where K is the curvature of the boundary in two dimensions. Note that there is no dependence on the form of the potential and that stationary boundaries have a planar shape. For a disk-shaped nucleus of radius R, $K = 1/R$ and integration of Eq. (4.1) yields

$$R^2(t) - R^2(0) = -2\gamma t \ . \tag{4.2}$$

In the MC simulations and in many experiments on systems with a nonconserved order parameter[1] the scaling of the dynamic structure factor with $t^{1/2}$ has been found as a consequence of Eq. (4.2). This implies that the boundary motion governs the dynamics of these systems on long distance and time scales.

In Fig. 8(a) the square of the radius of a circular nucleus is plotted as a function of discrete time for a 80×80 lattice of coupled cubic maps. The long-time behavior is linear and the measured slope is found to be in agreement with Eq. (4.2) to within 0.02%, for $\epsilon = 0.1$. Effects due to the discrete nature of the model were found for larger values of ϵ. Figure 8(b) shows $R^2(t)$ for $\epsilon = 0.3$; small-scale oscillations are superimposed on the linear decay. An explanation of the origin of these oscillations can be given easily. Consider the boundary structure along a radial line from the center of the nucleus. In the continuous case the one-dimensional boundary layer has a fixed shape in a reference frame moving with velocity v. However, in the discrete-space model the propagation is not smooth since the space is discrete and the boundary layer has to reorganize itself at each time step among the lattice sites in order to satisfy Eq. (4.2). Obviously this effect is stronger for

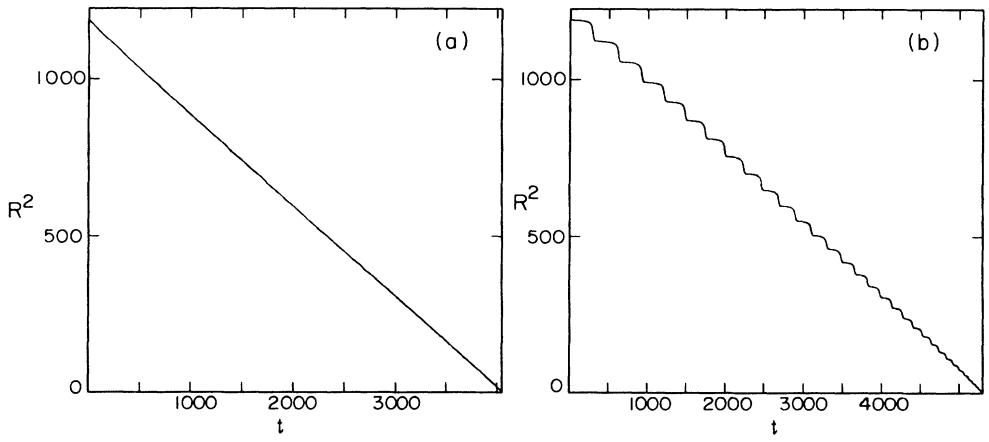

FIG. 8. Temporal evolution of the square of the radius of a circular nucleus for $\gamma = 0.15$, $c = 0$, (a) $\epsilon = 0.1$ and (b) $\epsilon = 0.3$.

sharper boundary layers, i.e., for larger values of the ϵ parameter. While the overall motion of the boundary may be a linear function of $t^{1/2}$, on a microscopic level the motion can be a periodic or more complex function of time. This aspect of the problem is currently under investigation.

A more important phenomenon occurs for small values of the diffusion constant γ. Figure 9 shows the critical value of γ for the stability of disk-shaped nuclei. In the shaded region, curved boundaries are found to be stable in disagreement with the Allen-Cahn theory. However, it is possible to avoid this problem, choosing a value of γ which guarantees instability of nuclei whose size is comparable with that of the system. For example, we have confirmed that any disk-shaped nucleus is unstable for $\gamma=0.15$ in a 100×100 coupled map lattice. This behavior is a consequence of the space discretization and does not depend on the particular form of the map.[14]

A further check of the Allen-Cahn theory entails the calculation of the dynamic structure factor, which is defined as

$$S(\mathbf{k},t)=\frac{1}{N}\sum_{j}\exp(i\mathbf{k}\cdot\mathbf{j})C(\mathbf{j},t)\ , \tag{4.3}$$

with N the number of coupled maps, and $C(\mathbf{i},t)$ is the correlation function given by

$$C(\mathbf{j},t)=\left\langle\sum_{j'}x(\mathbf{j}',t)x(\mathbf{j}'+\mathbf{j},t)\right\rangle\ . \tag{4.4}$$

The angular brackets signify an average over initial system states. In Fig. 10 the time evolution of one realization of the phase-separation process is shown for $\epsilon=0.2$, $\gamma=0.15$. The initial configuration was obtained by selecting $x(\mathbf{i},0)=0$, $\forall\mathbf{i}$ (the unstable state) and adding small-amplitude white noise.[15] The motion of the curved boundaries is evident. The structure factor was calculated by averaging over 60 different realizations of the phase-separation process and the results are reported in Fig. 11 where the function $\log_{10}[S(k,t)/t]$ is plotted as a function of $kt^{1/2}$. The $t^{1/2}$ scaling for all the allowed k values is satisfied for times longer than the time charac-

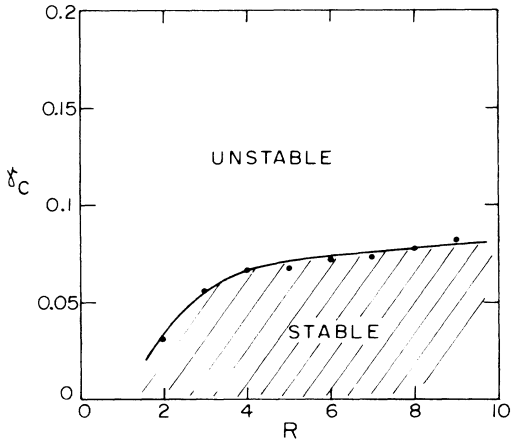

FIG. 9. Critical value γ_c for the stability of nuclei of radius R.

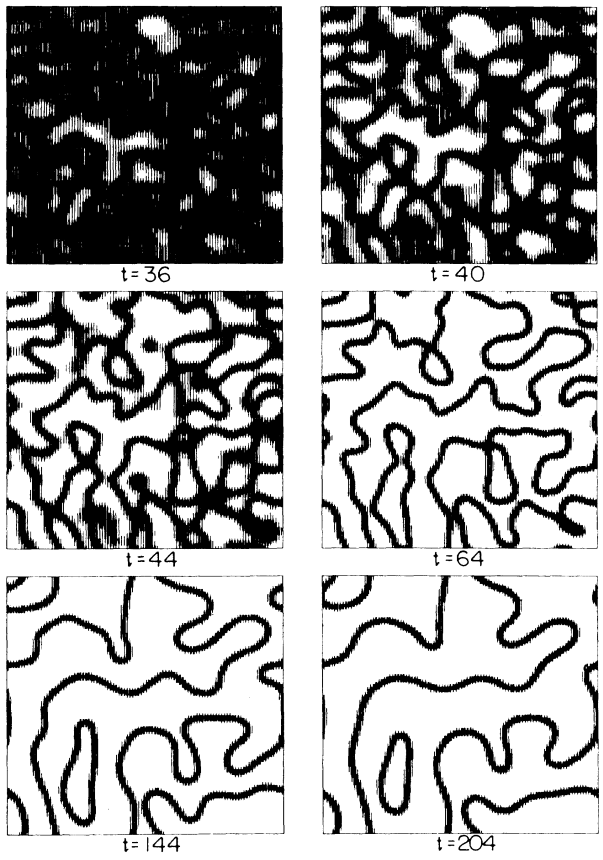

FIG. 10. Time evolution of a 100×100 coupled cubic map model for $\epsilon=0.2$, $c=0$, and $\gamma=0.15$. The color coding is chosen to emphasize deviations from the stable, homogeneous states and focus on the phase boundaries.

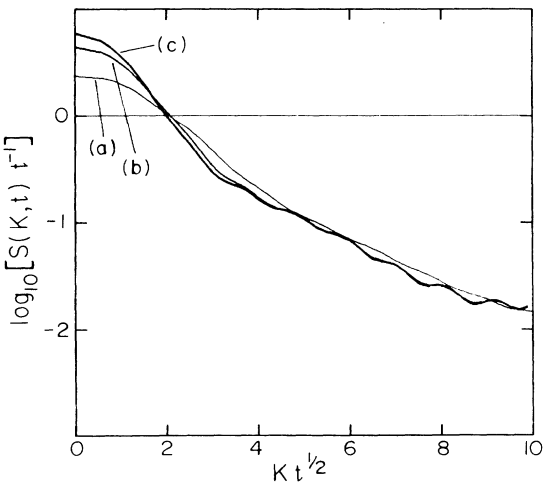

FIG. 11. Quantity $\log_{10}[S(k,t)/t]$ as a function of $kt^{1/2}$ for (a) $t=60$, (b) $t=110$, and (c) $t=160$. Note that at time $t=60$ the system has not yet relaxed to the Allen-Cahn regime. This picture can be compared with the analogous one of Ref. 17 where the theoretical prediction of Ref. 16 is also reported.

teristic of the relaxation to the stable states, and the shape of the structure factor is in agreement with theoretical predictions.[16] A comparison of this type was made earlier by Oono and Puri[17] for a system of coupled hyperbolic-tangent maps; however, our calculation shows that similar scaling results can be obtained with noninvertible maps with nearest-neighbor coupling. This obviates the need for a restriction to invertible discrete systems as suggested in Ref. 17. A stability analysis of the discrete model can provide information on the limited range of parameter values where effects specific to the discrete nature of the problem come into play.

Another test of the scaling behavior of the system can be made by studying the height of the peak in the structure factor at $k=0$ as a function of time.[18] This entails the calculation of the following quantity:

$$S(0,t)=N\left\langle \left[\frac{1}{N} \sum_{i=1}^{N} x(i,t) \right]^2 \right\rangle , \tag{4.5}$$

which not only yields information on the long-time evolution, but also on the initial development of ordered structures. The results of the simulations of $S(0,t)$ and $\log_{10}[S(0,t)/t]$ are reported in Fig. 12 for different values of ϵ.[19] Behavior on two different time scales can be observed in Fig. 12. The first time scale τ_0 characterizes the relaxation of the coupled map system towards the stable states. The second time scale corresponds to the end of the sharpening process for the boundaries separating the different phases; for times longer than τ_0 the boundary motion is described by the Allen-Cahn theory.

It is possible to give a simple description of the behavior of $S(0,t)$ for $t<\tau_0$. The dynamics is dominated by the exponential growth of the order parameter during the relaxation to the stable phases. Even for large values of γ the diffusion process has only a marginal effect on the temporal evolution. If one considers the extreme case of a lattice of decoupled ($\gamma=0$) cubic maps, the exponential growth of the behavior of the structure factor on the τ_0 time scale can be approximated by

$$S(0,t)\sim[f_L^{(t)}(\rho)]^2 , \tag{4.6a}$$

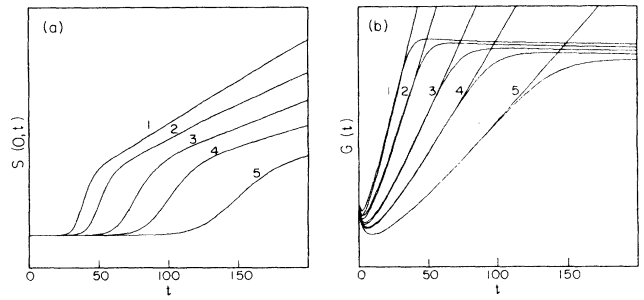

FIG. 12. Temporal evolution of the quantities (a) $S(0,t)$ and (b) $G(t)=\log_{10}[S(0,t)/t]$ for $\epsilon=0.2$ (1), $\epsilon=0.15$ (2), $\epsilon=0.1$ (3), $\epsilon=0.075$ (4), and $\epsilon=0.05$ (5). In panel (b) the early-stage curves obtained by Eq. (4.6) are also reported. The ordinate scale is arbitrary.

where $f_L(\rho)=(1+\epsilon)\rho$ is the linear approximation to the cubic map. The initial condition ρ in Eq. (4.6a) is an average quantity which takes into account the distribution of initial order parameter values near the unstable state:

$$\rho=\left[N\left\langle \left[\frac{1}{N} \sum_{i=1}^{N} \rho_i \right]^2 \right\rangle \right]^{1/2} . \tag{4.6b}$$

Here ρ_i is a random variable taken from the chosen noise distribution. For large N, ρ is just the standard deviation of the noise distribution.

The interpretation of the origin of the short-time ($t<\tau_0$) behavior of $S(0,t)$ is supported by comparison of Eq. (4.6) with results of simulations, which is presented in Fig. 12(b). A simple estimate of the time τ_0 may be obtained from the linear map $f_L(\rho)$ by computing the time it takes to reach some prescribed value C:

$$\tau_0=\frac{1}{\epsilon}\ln\left[\frac{C}{\rho} \right] . \tag{4.7}$$

The variation of τ_0 with ϵ^{-1} is confirmed by the results of simulations shown in Fig. 13.

We note that the evolution described by Eq. (4.6) is completely deterministic and is in agreement with Langevin equation simulations[15] in the limit of low temperatures. The behavior of the coupled map model in presence of noise and the connections with renormalization group theories[18] is presently under investigation.

V. NUCLEATION

Domain growth occurs by a different mechanism when c is not equal to zero. Due to the symmetric character of the cubic map, it is sufficient to examine positive values of c. Suppose c has a value close to the tangent boundary,

$$c=\pm 2\left[\frac{\epsilon}{3} \right]^{3/2} , \tag{5.1}$$

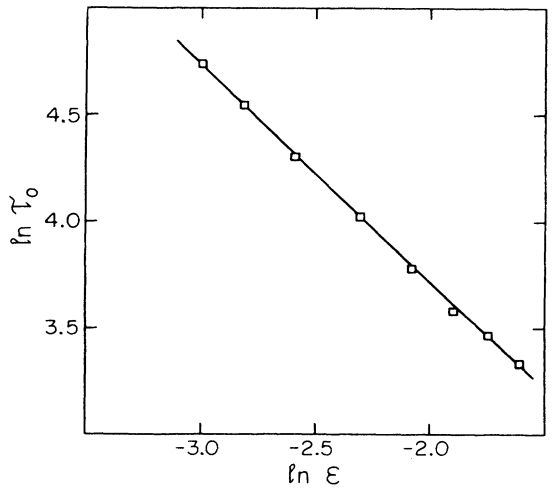

FIG. 13. τ_0 as a function of ϵ on a log-log scale. The straight line has a slope of -1.

in Fig. 1; there is a strong asymmetry in the quartic potential, and the unstable state lies close to one of the stable states. Consider an initial configuration in which seeds of the more-stable phase are randomly distributed in a sea of the less-stable state. When c is very close to the tangent boundary, perturbations of any size will grow. Figure 14 shows the time evolution for such a case when the initial probability of seeding p is equal to 0.005. The single-site perturbations form growing disk-shaped regions whose diameters increase at a nearly constant velocity v which is approximately equal to the propagation velocity of waves in the one-dimensional continuous case[3]:

$$v = -3x_0^* \sqrt{\gamma/2} \ , \tag{5.2}$$

where x_0^* is the unstable fixed point of the cubic map, Eq. (2.2). Although the measured propagation velocity is closely approximated by Eq. (5.2), there are systematic differences (cf. Fig. 15) which have their origin in the persistence of stationary solutions for small values of c for the discrete model.

A simple description of the nucleation growth can be accomplished by assuming that all lattice sites are in either one of the stable states. Clearly such a description implies a somewhat arbitrary classification of sites in the boundary layer as belonging to one of the two stable states. Introducing the subscript M (L) to represent the more (less) -stable state, the temporal evolution of the fraction of sites in the more stable state $N_M(t)$ can be described by the following approximate rate equation:

$$\frac{dN_M(t)}{dt} = \dot{A}(t)[1-N_M(t)] \ , \tag{5.3}$$

where $A(t)$ is the total surface area covered by the more-stable state, and $\dot{A}(t)$ is its time derivative. If each disk-shaped region grows linearly with time we have

$$A(t)=p\pi(R_0+vt)^2 \ , \tag{5.4}$$

where R_0 is the initial radius of a seed of the more-stable state. Equation (5.3) simply expresses the fact that the rate of growth of regions of the more-stable phase is proportional to the intrinsic growth rate of the seeds times the fraction of sites which remain in the less-stable phase. Substituting Eq. (5.4) in (5.3) and integrating, we obtain

$$N_M(t)=1-(1-\pi pR_0^2)\exp[-\pi pv(2R_0t+vt^2)] \ , \tag{5.5}$$

which contains the exponential dependence characteristic of a nucleation process.[3] A similar law was obtained

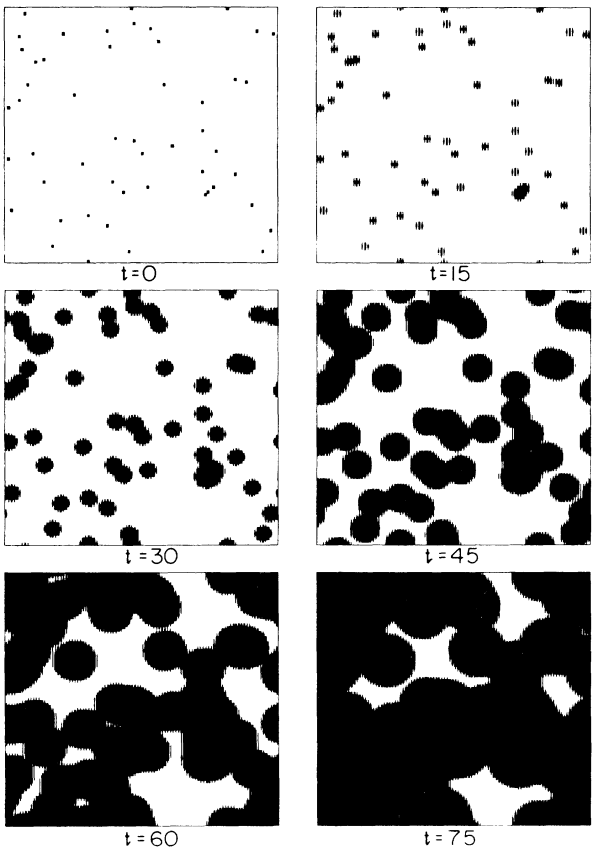

FIG. 14. Temporal evolution of a 100×100 coupled cubic map lattice for $\epsilon=0.3$, $c=0.063$, and $\gamma=0.15$. The black (white) color corresponds to the more (less) -stable phase. The initial state is given by seeding the uniform less-stable state with the more-stable state with probability $p=0.005$.

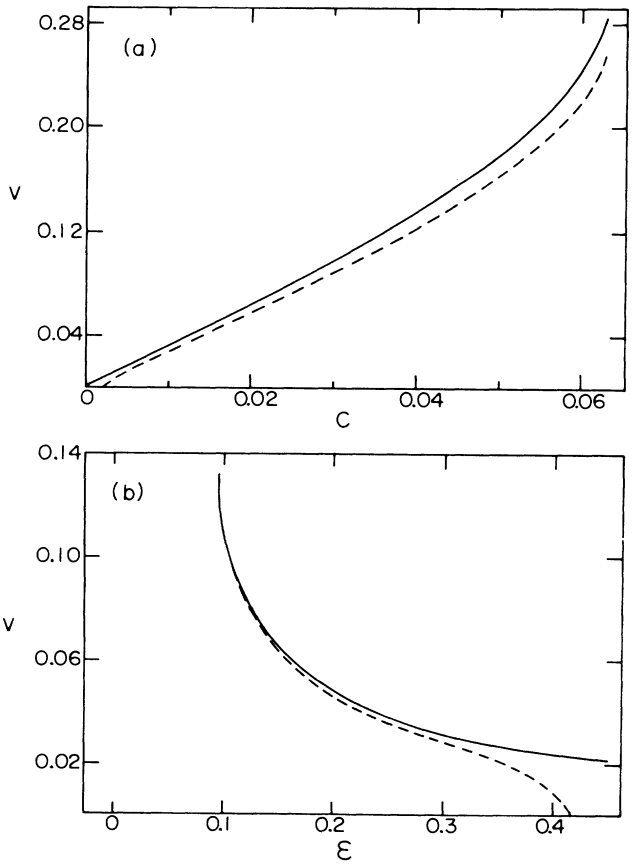

FIG. 15. Comparison between simulations of the cubic map lattice (dashed line) and Eq. (5.2) (solid line), for the velocity v of a one-dimensional kink for (a) $\gamma=0.2$ and $\epsilon=0.3$ and (b) $\gamma=0.2$ and $c=0.1$.

in the context of ring propagation in an excitable medium.[20,21] In the excitable-medium cellular automaton, the velocity of propagation is unity and does not appear explicitly in the calculation.

One can use Eq. (5.5) to approximately calculate quantities averaged over the lattice, and we again focus on the $k=0$ value of the structure factor, $S(0,t)$. Letting x_L and x_M be the values of the order parameter in the less- and more-stable states, respectively, one obtains

$$S(0,t)=N[N_M x_M + x_L(1-N_M)]^2 , \tag{5.6}$$

which exhibits a minimum for

$$\hat{N}_M = \frac{-x_L}{(x_M - x_L)} \tag{5.7}$$

at the time $\hat{t}$ given by

$$\hat{t} = -\frac{R_0}{v} + \left[\frac{R_0^2}{v^2} - \frac{1}{\pi p v^2} \ln \left[\frac{x_L}{(x_M - x_L)(1-\pi p R_0^2)} \right] \right]^{1/2} . \tag{5.8}$$

The time $\hat{t}$ will be positive provided

$$R_0 < \left[\frac{\hat{N}_M}{\pi p} \right]^{1/2} , \tag{5.9}$$

which relates the initial radius of a nucleus with the seeding probability p.

Since the mean-field theory outlined above assumes that all order-parameter states on the lattice can be classified as belonging to either of the stable states, its validity is restricted to large values of the parameter ϵ where the boundary layer is sharp. However, Eq. (5.5) provides a good approximation to the dynamics even in the case of small ϵ. A comparison between the theory and the simulation is shown in Fig. 16 for the case of $p=0.005$. The theory will fail for large p due to correlation effects; the growth of a site will be delayed or accelerated depending on its neighbors. In Fig. 17 the form of the map $x(\mathbf{i},t)$ and of its first nearest neighbor $x(\mathbf{j},t)$ are shown in the case of a single-site perturbation. Even if the late-stage dynamics corresponds to disk growth, the perturbation initially shrinks until the feedback influence of the nearest neighbors vanishes. This corresponds to a "tangent" behavior of iterates of the first-nearest-neighbor map, which spend many time steps in the vicinity of the near-tangency. At a critical value $c_{\rm crit}$ of the parameter c (~ 0.0624 for $\gamma=0.1$), the behavior of the perturbed site and its neighbors is exchanged; the single-site disturbance is then absorbed by the sea of the less-stable phase through a tangent mechanism. For values of c larger than $c_{\rm crit}$, the dynamics is well approximated by the two-dimensional system:

$$\begin{aligned} x(\mathbf{i},t+1) &= f(x(\mathbf{i},t)) + 4\gamma[x(\mathbf{j},t) - x(\mathbf{i},t)] , \\ x(\mathbf{j},t+1) &= f(x(\mathbf{j},t)) + \gamma[x(\mathbf{i},t) - x(\mathbf{j},t)] , \end{aligned} \tag{5.10}$$

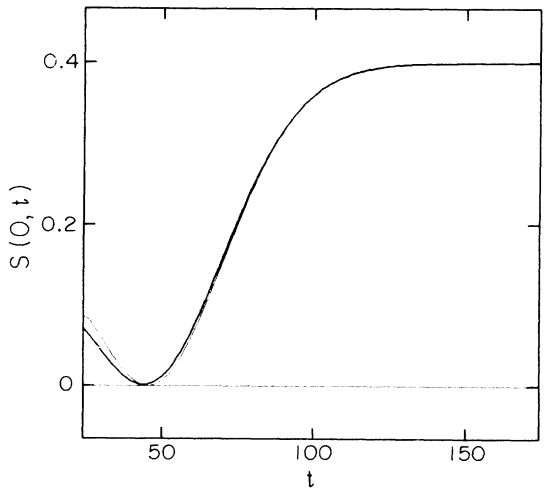

FIG. 16. Structure factor $S(0,t)$ (divided by N) for the nucleation dynamics shown in Fig. 14. The thick line represents the simulation on a 100×100 cubic map lattice, averaged over 30 initial realizations; the thin line is the theoretical result, Eq. (5.6). The initial time is set equal to τ_d. Note the initial discrepancy due to discretization effects.

which assumes a homogeneous structure of the lattice around the perturbation. By using this two-dimensional map, one can approximately evaluate the delay time τ_d which it takes the perturbed site to reestablish the initial value of the order parameter. For example, in the case of Fig. 16, τ_d is found to be approximately 25 time iterations. However, for values of c closer to $c_{\rm crit}$, τ_d diverges and the two-dimensional description given by Eq. (5.10) breaks down. The fate of the single-site perturbation is then affected by the behavior of the second or third nearest neighbors and a larger system of coupled maps is necessary to describe the dynamics. Obviously, in the case of two-site perturbations the delay time τ_d is shortened and the nucleus will start to grow earlier than in the case of an isolated seed. In the case of a large probability of seeding, initial coexistence of seeds of different sizes is possible, giving rise to a more complex temporal evolution; Eq. (5.3) is not valid in this case. However, this effect is reduced if the initial seeds have a size R_0 larger than one lattice spacing.

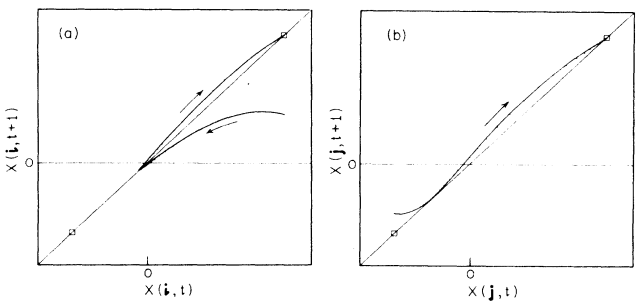

FIG. 17. Initial dynamics of a single-site perturbation of the more-stable state in a sea of the less-stable state for the perturbed map $x(\mathbf{i},t)$ (a) and for its first-nearest-neighbor map $x(\mathbf{j},t)$ (b). The arrows indicate the direction of evolution.

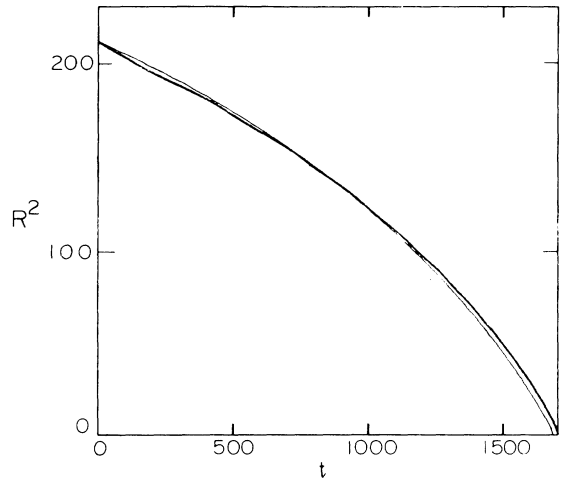

FIG. 18. Temporal evolution of the square of the radius of a disk-shaped nucleus for $\gamma=0.15$, $\epsilon=0.1$, and $c=0.001$ (thick line) compared with the results of Eq. (5.13) (thin line).

A different situation is found for values of c far from the tangent boundary, Eq. (5.1). In this case the size of the initial nucleus has to exceed a critical value in order for growth of the nucleus to occur. This situation has been extensively studied in the past[3] and estimates of the critical radius R_c of the nucleus have been given. Here we study nucleation phenomena in the discrete model and compare the results with some of the theoretical predictions; we concentrate especially on dynamical aspects of the nucleation process. A simple estimate of the critical radius which is based on continuous-time dynamics can be determined in the following way. Consider a disk-shaped nucleus of radius R of the more-stable phase embedded in a sea of the less-stable phase. The curvature the nucleus gives rise to contraction (cf. Sec. IV), which is counterbalanced by a linear growth due to the different stabilities of the two phases; thus,

$$\dot{R}=-\frac{\gamma}{R}+v \ , \tag{5.11}$$

where the velocity v is given by Eq. (5.2) if the nucleus is large enough. Hence, the critical radius R_c is[3]

$$R_c=\frac{\gamma}{v} \ . \tag{5.12}$$

Here, we are more interested in the dynamical effects. Upon integration of Eq. (5.10), one has

$$t=\frac{1}{v}\left[R-R_0+R_c \ln\left[\frac{R-R_c}{R_0-R_c}\right]\right] , \tag{5.13}$$

which can describe both shrinking and growing of the nucleus, depending on the initial condition. Figure 18 shows a comparison between Eq. (5.13) and the simulation for the case of shrinking nuclei. Analogous agreement has been found for the growing case.

The above results establish the usefulness of the cubic map lattice for studies of nucleation growth in systems with nonconserved order parameter. This case is especially important in view of the fact that some chemical systems, like the iodate-arsenous acid system,[22] are of this type, and are thus amenable to study through the use of discrete models.

VI. DISCUSSION

The results presented in this paper have shown that coupled map lattices exhibit interesting phase-separation phenomena when the isolated maps comprising the lattice possess bistable steady states. As for their continuum counterparts, the dynamics of domain boundaries separating equivalent states obeys Allen-Cahn scaling for long times, while domain growth or shrinkage occurs by a nucleation mechanism when the states are not equivalent. The discrete nature of the model can have important consequences in some circumstances, for example, the existence of stationary boundaries separating inequivalent states for certain parameter ranges. Nonetheless, with a suitable rescaling of system parameters the model faithfully represents most features of the phase-separation process, and is attractive due to its simplicity and ability to be simulated easily.

This class of models can be extended to investigate other related phenomena. Systems with more than a single order parameter present interesting features, especially those connected with the structure of the discrete stationary interface, since several stable and unstable manifolds enter the description. Discrete models of this type often appear in biological applications, where more complex phenomena may occur.[7] There may be coexistence of more than two stable homogeneous states, and the coexisting states need not be simple stationary states. The phase structure and dynamics can be investigated using the techniques presented in this paper.

ACKNOWLEDGMENTS

We would like to thank C. Baesens, P. Bak, E. Celarier, M.-N. Chee, Y. Elskens, S. Fraser, V. Pokrovsky, and A. Politi for useful discussions. This work is partially supported by a grant from the Natural Sciences and Engineering Research Council of Canada.

[1]J. D. Gunton, M. San Miguel, and P. S. Sahni, in *Phase Transition and Critical Phenomena*, edited by C. Domb and J. L. Lebowitz (Academic, New York, 1983), Vol. 8, p. 267.

[2]S. M. Allen and J. W. Cahn, Acta Metall. **27**, 1085 (1979).

[3]F. Schlögl, Z. Phys. **253**, 147 (1972); F. Schlögl and R. S. Berry, Phys. Rev. A **21**, 2078 (1980); A. Nitzan, P. Ortoleva, and J. Ross, Faraday Symp. Chem. Soc. **9**, 241 (1974); F. F. Abraham, *Homogeneous Nucleation Theory* (Academic, New

York, 1974); A. M. Albano, N. B. Abraham, D. E. Chyba, and M. Martelli, Am. J. Phys. **52**, 161 (1983).

[4]S. Wolfram, *Theory and Applications of Cellular Automata* (World Scientific, Singapore, 1986).

[5](a) I. Waller and R. Kapral, Phys. Rev. A **30**, 2047 (1984); R. Kapral, *ibid.* **31**, 3868 (1985); G.-L. Oppo and R. Kapral, *ibid.* **33**, 4219 (1986); (b) K. Kaneko, Prog. Theor. Phys. **69**, 1427 (1983); **72**, 480 (1984); **74**, 1033 (1985); (c) J. D. Keeler and J. D. Farmer, Physica D **23**, 413 (1986).

[6]R. Kapral, and G.-L. Oppo, Physica D **23**, 455 (1986).

[7]See, for instance, J. J. Bull, C. Thompson, D. Ng, and R. Moore, Am. Nat. **129**, 143 (1987); M. Rotenberg (unpublished); R. Kapral, G.-L. Oppo, and D. B. Brown, Physica A (to be published).

[8]In order to compare the dynamics of the discrete model with that of the continuous equation we note that under a suitable rescaling of the time, space, and order parameter one can always obtain values of ϵ and c that lie inside the shaded region of Fig. 1. Moreover, such a scaling provides an estimate of the magnitude of the discrete time unit and lattice spacing.

[9]P. Bak and V. L. Pokrovsky, Phys. Rev. Lett. **47**, 958 (1981); S. Aubry and P. Y. Le Daeron, Physica D **8**, 381 (1983); V. L. Pokrovsky, J. Phys. (Paris) **42**, 761 (1981); S. E. Burkov, V. L. Pokrovsky, and G. Uimin, J. Phys. A **15**, L645 (1982).

[10]E. M. McMillan, in *Topics in Modern Physics* (Colorado University Press, Boulder, 1971), p. 219.

[11]E. Shöll, Z. Phys. B **62**, 245 (1986).

[12]However, there are limitations on the precision that can be obtained: If a precision of order 10^{-m} for the intersection with the chosen surface is required, the corresponding correction $\delta \mathbf{r}$ on the starting point must be of order $(\lambda_+)^{-n}10^{-m}$, and can easily surpass the precision of the computer. For example, for $n=11$, and working in double precision, we could go no further than $m=8$ in the chosen range of values of ϵ. Obviously, one can reduce the number of iterations n but the linear approximation in the neighborhood of the fixed point may no longer be valid.

[13]Note that the circle at (0,0) of that figure is due to a misprint in the plot.

[14]Since some authors have suggested the equivalence of coupled map models with dynamical Ising models [T. Bohr, G. Grinstein, Y. He, and C. Jayaprakash, Phys. Rev. Lett. **58**, 2155 (1987)], it may be interesting to show that phenomena like stable nuclei can be found in Ising models as well.

[15]This corresponds to the choice (iii) of O. T. Valls and G. F. Mazenko, Phys. Rev. B **34**, 7941 (1986).

[16]T. Ohta, D. Jasnow, and K. Kawasaki, Phys. Rev. Lett. **49**, 1223 (1982).

[17]Y. Oono and S. Puri, Phys. Rev. Lett. **58**, 836 (1987).

[18]G. F. Mazenko and O. T. Valls, Phys. Rev. B **27**, 6811 (1983); **30**, 6732 (1984); E. T. Gawlinski, M. Grant, J. D. Gunton, and K. Kaski, *ibid.* **31**, 281 (1985).

[19]The simulations required only 20 min of CPU (central processing unit) time on a Gould 32/9705 computer for a lattice of 100×100 cells, 200 time steps, and 30 realizations of the phase-separation process.

[20]S. Fraser and R. Kapral, J. Chem. Phys. **85**, 5682 (1986).

[21]R. M. Bradley, J. Chem. Phys. **86**, 7245 (1987).

[22]A. Saul and K. Showalter, in *Oscillations and Traveling Waves in Chemical Systems,* edited by R. J. Field and M. Burger (Wiley, New York, 1985), p. 419, and references therein.